

## Article

# Fabricating Spinel-Type High-Entropy Oxides of (Co, Fe, Mn, Ni, Cr)<sub>3</sub>O<sub>4</sub> for Efficient Oxygen Evolution Reaction

Xiaofei Hao <sup>1,\*</sup>, Ran Wang <sup>2</sup>, Xiumin Tan <sup>1</sup>, Xiufeng Zhang <sup>1</sup>, Xupo Liu <sup>2,\*</sup>, Zhaoyang Wu <sup>1</sup> and Dongli Yuan <sup>1</sup>

<sup>1</sup> Zhengzhou Institute of Multipurpose Utilization of Mineral Resources, Chinese Academy of Geological Sciences, Zhengzhou 450006, China; zzs\_tan@163.com (X.T.); zh200318@126.com (X.Z.); wzy500@sina.com (Z.W.); yuandongli99@163.com (D.Y.)

<sup>2</sup> School of Materials Science and Engineering, Henan Normal University, Xinxiang 453007, China; 2125283034@stu.htu.edu.cn

\* Correspondence: haopaper@163.com (X.H.); liuxupo@htu.edu.cn (X.L.);  
Tel.: +86-19837166511 (X.H.); +86-15907164432 (X.L.)

**Abstract:** Fabricating efficient oxygen evolution reaction (OER) electrocatalysts is crucial for water electrocatalysis. Herein, the spinel-type high-entropy oxides of (Co, Fe, Mn, Ni, Cr)<sub>3</sub>O<sub>4</sub> were synthesized through the high-temperature calcination approach. The influences of calcination temperatures on structures and electrochemical properties were investigated. The optimized catalyst of HEO-900 contains the hybrid structure of regular polyhedrons and irregular nanoparticles, which is beneficial for the exposure of electrochemically active sites. It was identified that the abundant high-valence metal species of Ni<sup>3+</sup>, Co<sup>3+</sup>, Fe<sup>3+</sup>, Mn<sup>4+</sup>, and Cr<sup>3+</sup> are formed during the OER process, which is generally regarded as the electrochemically active sites for OER. Because of the synergistic effect of multi-metal active sites, the optimized HEO-900 catalyst indicates excellent OER activity, which needs the overpotential of 366 mV to reach the current density of 10 mA cm<sup>-2</sup>. Moreover, HEO-900 reveals the prominent durability of running for 24 h at the current density of 10 mA cm<sup>-2</sup> without clear delay. Therefore, this work supplies a promising route for preparing high-performance multi-metal OER electrocatalysts for water electrocatalysis application.

**Keywords:** spinel type high-entropy oxides; electrocatalyst; oxygen evolution reaction; water splitting

**Citation:** Hao, X.; Wang, R.; Tan, X.; Zhang, X.; Liu, X.; Wu, Z.; Yuan, D. Fabricating Spinel-Type High-Entropy Oxides of (Co, Fe, Mn, Ni, Cr)<sub>3</sub>O<sub>4</sub> for Efficient Oxygen Evolution Reaction. *Materials* **2024**, *17*, 3415. <https://doi.org/10.3390/ma17143415>

Academic Editor: Hiroaki Onoda

Received: 4 June 2024

Revised: 30 June 2024

Accepted: 8 July 2024

Published: 10 July 2024



**Copyright:** © 2024 by the authors. Licensee MDPI, Basel, Switzerland. This article is an open access article distributed under the terms and conditions of the Creative Commons Attribution (CC BY) license (<https://creativecommons.org/licenses/by/4.0/>).

## 1. Introduction

Water electrolysis is a promising strategy for producing clean and renewable hydrogen energy fuel through employing sustainable solar and wind energy [1–3]. During the electrolysis process, the oxygen evolution reaction (OER) is a crucial step as it determines the overall efficiency and performance of the electrolyzer [4,5]. Thus, research on high-performance OER catalysts for water electrolysis is of great significance. Generally, efficient and cost-effective OER catalysts are essential to improve the kinetics of oxygen evolution, reduce energy consumption, and enhance the overall electrolyzer performance [6,7]. Recent advances have reported large numbers of electrocatalysts for OER applications [8,9]. However, taking both the prominent activity and durability of OER catalysts into consideration at the same time is still a huge challenge.

There are many compounds being investigated for OER, such as transition metal-based hydroxides [7], oxides [10], phosphides [11,12], sulfides [13–15] and nitrides [16]. Among them, spinel oxides (AB<sub>2</sub>O<sub>4</sub>) have been widely used as an electrocatalyst for oxygen evolution due to their diverse and adjustable electronic structure and properties [17]. The development of spinel-type catalysts for OER has gained significant attention in the field of electrocatalyst exploration [18]. Over the years, extensive efforts have been made to optimize the composition and structure of spinel catalysts. Different synthesis techniques, including sol-gel, hydrothermal, and solid-state methods, have been em-

ployed to fabricate catalysts with desirable properties [19]. The addition of various dopants or nanoscale modifications has also been explored to improve catalytic performance. However, the electrocatalytic properties of spinel-type catalysts are still inferior to precious metal-based catalysts ( $\text{RuO}_2$  and  $\text{IrO}_2$ ) [20]. Fortunately, the construction of high-entropy oxides is an efficient approach to enhance the electrochemical performances of spinel oxides. High-entropy oxides are a series of compounds with five or more different species with equal atomic ratios [21,22]. Taking the prominent advantage of the high-entropy synergetic effect of multiple metallic oxides is beneficial for tailoring the electronic structures and OER catalytic activity of spinel-type oxides.[21] In addition, spinel-type high-entropy oxides always possess high electrochemical durability due to the high-entropy stabilization effect [23,24]. However, the high-entropy alloy nanoparticles always contain four or more elements, and the problem of low-product purity easily occurs, hindering their application in the electrocatalytic system.

In this work, the wet ball-milling and following high-temperature calcination were adopted to synthesize the spinel-type high-entropy oxides of  $(\text{Co}, \text{Fe}, \text{Mn}, \text{Ni}, \text{Cr})_3\text{O}_4$ . The wet ball-milling treatment could effectively promote the full mixing of raw material powders, which is conducive to the formation of high-purity, high-entropy oxides in the calcination process. The optimized catalyst displays the special hybrid structure of regular polyhedrons and irregular nanoparticles, which promotes the exposure of electrochemically active sites. Owing to the synergistic effect of the multi-metal sites, the as-prepared HEO-900 catalyst indicates excellent OER activity of just needing the overpotential of 366 mV to reach the current density of  $10 \text{ mA cm}^{-2}$ . In addition, the HEO-900 catalyst exhibits prominent durability when running for 24 h at the current density of  $10 \text{ mA cm}^{-2}$  with clear delay. Therefore, this work supplies a promising route for preparing high-performance multi-metal OER electrocatalysts for water electrocatalysis application.

## 2. Materials and Methods

### 2.1. Materials

The raw materials of  $\text{Co}_2\text{O}_3$ ,  $\text{Fe}_2\text{O}_3$ ,  $\text{Mn}_2\text{O}_3$ ,  $\text{Ni}_2\text{O}_3$ , and  $\text{Cr}_2\text{O}_3$  with AR purity were all purchased from Tianjin Kemiou Chemical Reagent Co., Ltd. (Tianjin, China). KOH (85%) was obtained from Shanghai Aladdin Bio-Chem Technology Co., Ltd. (Shanghai, China). Carbon cloth was obtained from the Kunshan Tengerhui Co., Ltd. (Kunshan, China). Deionized water was applied to dispense the electrolyte solution.

### 2.2. Electrocatalyst Preparation

The spinel-type high-entropy oxides of  $(\text{Co}, \text{Fe}, \text{Mn}, \text{Ni}, \text{Cr})_3\text{O}_4$  were synthesized through the high-temperature calcination method. Firstly, 0.2 mol  $\text{Co}_2\text{O}_3$ , 0.2 mol  $\text{Fe}_2\text{O}_3$ , 0.2 mol  $\text{Mn}_2\text{O}_3$ , 0.2 mol  $\text{Ni}_2\text{O}_3$ , and 0.2 mol  $\text{Cr}_2\text{O}_3$  were ground with alcohol as the grinding medium for 3 h. Then, the mixtures were heated up to the temperature of  $x \text{ }^\circ\text{C}$  for 4 h with a heating rate of  $5 \text{ }^\circ\text{C min}^{-1}$  in an air atmosphere. After cooling down to room temperature, the obtained catalysts were named HEO- $x$ , where  $x$  represented the heating temperature of 800, 900, 1000, and 1100  $^\circ\text{C}$ , respectively. For comparison, the raw materials of oxide mixtures were also applied as the HEO-O catalyst.

### 2.3. Physical Characterization

The X-ray diffraction (XRD) patterns of the prepared electrocatalysts were performed through a Dutch Empyrean in situ electrochemical X-ray diffractometer with CuK $\alpha$  as the radiation source. The morphologies of catalysts were achieved on the Regulus8220 field emission scanning electron microscope (FESEM) and the JEOL JEM-2100 transmission electron microscope (TEM) equipped with energy-dispersive X-ray spectrum (EDS). The surface elemental compositions and element valences of samples were exploited via the Thermo Scientific (Waltham, MA, USA) K-Alpha X-ray photoelectron spectroscopy (XPS).

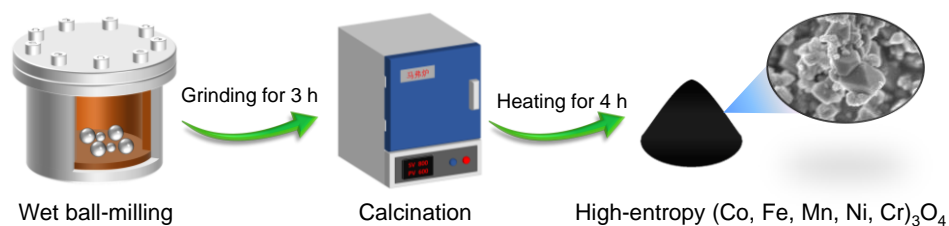
## 2.4. Electrochemical Determinations

In this work, all the electrochemical determinations were carried out in a 1.0 M KOH electrolyte via a three-electrode system based on the CHI660E electrochemical workstation (Chenhua). To achieve the working electrode, 10 mg of the prepared catalyst, modified Kaolin and graphene (5:2:3) was uniformly dispersed in a 2 mL 0.1% Nafion/isopropanol solution through ultrasonic treatment. Then, 100  $\mu$ L of the obtained ink was dropped on the treated carbon paper and dried to obtain the working electrode. The graphite rod and Hg/HgO electrode were employed as the counter electrode and reference electrode, respectively. All the potentials were revised according to the reversible hydrogen electrode (RHE) through the equation  $E(\text{RHE}) = E(\text{Hg/HgO}) + 0.0591 \times \text{pH} + 0.098 \text{ V}$ . Linear sweep voltammetry (LSV) curves of catalysts were detected in the voltage range of 1.0–1.8 V at a scan rate of 5  $\text{mV s}^{-1}$ . To evaluate the durability, the chronopotentiometric curve of HEO-900 was determined at the current density of 10  $\text{mA cm}^{-2}$ . The double-layer capacitance was estimated by cyclic voltammetry in the range of 0.75–0.85 V with sweep rates of 10, 20, 40, 60, 80, and 100  $\text{V s}^{-1}$ . Electrochemical impedance spectroscopy (EIS) data were determined in the frequency range of 0.1 MHz–0.01 Hz.

## 3. Results

### 3.1. Structure Characterization

The spinel-type high-entropy oxides of  $(\text{Co, Fe, Mn, Ni, Cr})_3\text{O}_4$  in this work were synthesized through the wet ball-milling and following high-temperature calcination, as shown in Scheme 1. The wet ball-milling treatment is believed to promote the sufficient mixing of raw material powders and thus accelerates the formation of high-entropy oxides in the calcination process. The obtained catalysts were named HEO- $x$ , where  $x$  represents the heating temperature of 800, 900, 1000, and 1100  $^{\circ}\text{C}$ , respectively. Firstly, the phase compositions of catalysts were determined and analyzed. The raw material mixture of HEO-0 displays the tanglesome XRD peaks, as shown in Figure 1a. The XRD peaks of  $\text{Co}_2\text{O}_3$ ,  $\text{Fe}_2\text{O}_3$ ,  $\text{Mn}_2\text{O}_3$ ,  $\text{Ni}_2\text{O}_3$ , and  $\text{Cr}_2\text{O}_3$  can be observed and consist of a composition of raw materials. After the calcination process, the XRD peaks changed significantly. All the samples of HEO-800, HEO-900, HEO-1000 and HEO-1100 showed similar XRD peaks located at  $18.27^{\circ}$ ,  $30.17^{\circ}$ ,  $35.59^{\circ}$ ,  $37.20^{\circ}$ ,  $43.28^{\circ}$ ,  $53.76^{\circ}$ ,  $57.33^{\circ}$ ,  $62.97^{\circ}$  and  $74.56^{\circ}$ , as shown in Figure 1b. These peaks are identical to the standard characteristic peaks of  $\text{CoFe}_2\text{O}_4$  (PDF 03-0864), revealing the single spinel phase. There is no peak belonging to the other oxides observed. Thus, the introduction of other metal elements (Ni, Mn, and Cr) clearly does not change the original crystal structure of the  $\text{CoFe}_2\text{O}_4$  phase. According to the above result, we think that the as-synthesized high-entropy oxides of  $(\text{Co, Fe, Mn, Ni, Cr})_3\text{O}_4$  display a cubic phase crystal structure with the lattice parameter of  $a = 8.377 \text{ \AA}$ , similar to that of  $\text{CoFe}_2\text{O}_4$  (PDF#03-0864). The XRD result preliminarily confirms the successful fabrication of high-entropy  $(\text{Co, Fe, Mn, Ni, Cr})_3\text{O}_4$  oxides with a single cubic spinel phase. In addition, it is notable that the XRD peak intensity of the catalysts shows an enhanced trend as the calcination temperatures increase, proving the promoted crystallinity of these high-entropy oxides.



**Scheme 1.** The synthesis process diagram of preparing the spinel-type high-entropy oxides of  $(\text{Co, Fe, Mn, Ni, Cr})_3\text{O}_4$ .

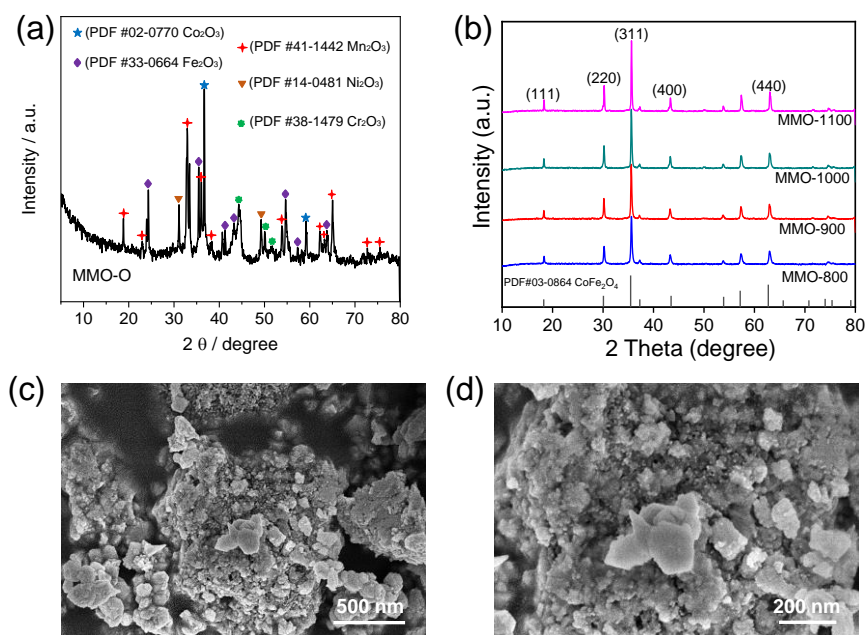


**Figure 1.** (a) XRD pattern of the raw material mixture. (b) XRD patterns of the prepared HEO-800, HEO-900, HEO-1000 and HEO-1100 catalysts. (c,d) SEM images of HEO-O.

SEM images were detected to exploit the microstructure of the prepared electrocatalysts. The SEM images of HEO-O in Figure 1c,d indicate that the raw material mixture consists of some irregular grains with different sizes. However, the morphologies were clearly changed after the high-temperature calcination process, as shown in Figure 2a–h. It was found that there are some regular polyhedrons formed in these catalysts during the calcination process, and the percentages of polyhedrons are promoted as the calcination temperatures increase. The HEO-800 sample that is calcined at 800 °C still contains many irregular nanograins (Figure 2a,b). As the calcining temperature increases up to 900 °C, the number of irregular nanoparticles further decrease, and more polyhedrons are generated. The HEO-900 electrocatalyst shows the structure of regular polyhedrons with a small quantity of irregular nanoparticles (Figure 2c,d). When the temperatures further increase to 1000 °C and 1100 °C, the synthesized HEO-1000 and HEO-1100 samples mainly display the morphology of regular polyhedrons (Figure 2e–h). Thus, the calcination temperatures have an important effect on the microstructures of high-entropy (Co, Fe, Mn, Ni, Cr)<sub>3</sub>O<sub>4</sub> electrocatalysts. In general, regular polyhedrons contain high degrees of crystallinity, which are damaging for promoting the exposure of electrochemically active sites. However, the hybrid structure of regular polyhedrons and irregular nanoparticles may be beneficial for achieving excellent OER activity.

The TEM images of the HEO-900 sample have also been determined to analyze the structure, as shown in Figure 2i–l. It can be seen that HEO-900 consists of some regular polyhedrons and irregular nanoparticles (Figure 2i–l), matching well with the SEM analysis. The lattice fringes with a lattice distance of 0.473 nm correspond to the (111) facet of the CoFe<sub>2</sub>O<sub>4</sub> phase (Figure 2k). The mapping images indicate the uniform dispersion of Co, Fe, Mn, Ni, Cr, and O around the polyhedron (Figure 2l), further proving the successful fabrication of the spinel-type high-entropy (Co, Fe, Mn, Ni, Cr)<sub>3</sub>O<sub>4</sub> electrocatalyst. The uniform dispersion of metal atoms is conducive to achieving the synergistic effect of multiple metal sites, which is expected to enhance the OER performances.

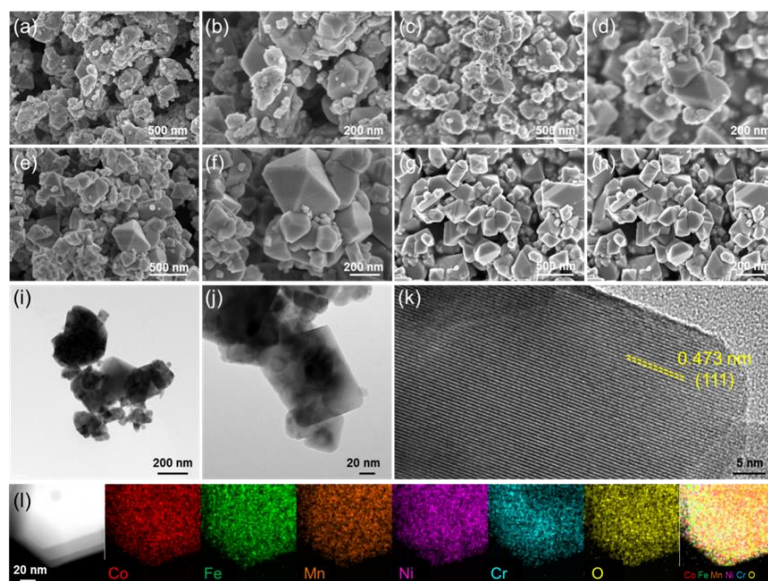


**Figure 2.** SEM images of (a,b) HEO-800, (c,d) HEO-900, (e,f) HEO-1000, (g,h) HEO-1100. TEM images of HEO-900: (i,j) TEM images, (k) high-resolution TEM images, and (l) elemental mapping images of Co, Fe, Mn, Ni, Cr, and O.

### 3.2. Electrocatalytic Performances

The electrocatalytic performances of the high-entropy (Co, Fe, Mn, Ni, Cr)<sub>3</sub>O<sub>4</sub> catalysts were determined in 1.0 M KOH through the common three-electrode system. Figure 3a shows the OER polarization curves of the prepared catalysts. It can be observed that the HEO-900 electrocatalyst displays the best OER activity among these samples. To achieve the current density of 10 mA cm<sup>-2</sup>, HEO-900 just needs the overpotential of 366 mV, which is much lower than those of HEO-O (425 mV), HEO-800 (398 mV), HEO-1000 (412 mV), and HEO-1100 (460 mV), as shown in Figure 3b. In addition, the Tafel slopes of HEO-O and HEO-900 calculated from the LSV curves were adopted to evaluate the OER activity (Figure 3c). It was found that the HEO-900 electrocatalyst possesses a lower Tafel slope of 76.35 mV dec<sup>-1</sup> than HEO-O (118.34 mV dec<sup>-1</sup>), revealing a faster OER reaction mechanism and better catalytic activity. We compared the OER performances of HEO-900 with the recently reported catalysts, as shown in Table S1 [25–36]. It is notable that HEO-900 displayed compatible performances with the reported catalysts, revealing promising applications. The excellent OER activity of the high-entropy (Co, Fe, Mn, Ni, Cr)<sub>3</sub>O<sub>4</sub> catalyst is due to the synergetic effect of multiple metal sites. In addition, durability is also important for the OER electrocatalysts. The chronopotentiometric curve of HEO-900 was determined at the constant current density of 10 mA cm<sup>-2</sup>, as shown in Figure 3d. It can be seen that there was no clear delay to the applied potential, proving that the as-synthesized HEO-900 sample had prominent operation durability. The high durability is attributed to the high-entropy stabilization effect of the (Co, Fe, Mn, Ni, Cr)<sub>3</sub>O<sub>4</sub> catalysts. The above-mentioned results confirm that the as-prepared HEO-900 sample contains excellent OER activity and operating durability.

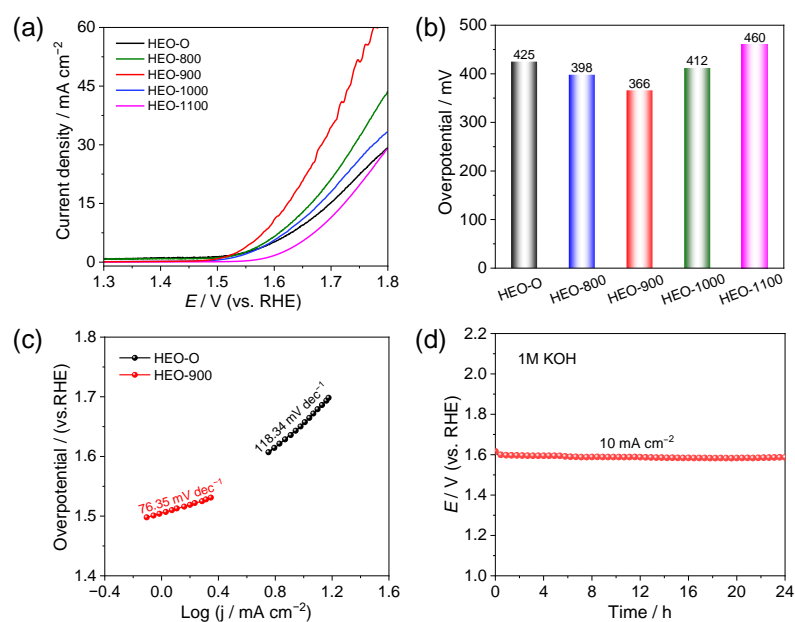


**Figure 3.** (a) OER polarization curves of the prepared catalysts. (b) Comparison of the overpotentials at the current density of 10 mA cm<sup>-2</sup>. (c) Tafel slopes of HEO-O and HEO-900. (d) The chronopotentiometric curve of HEO-900 at the constant current density of 10 mA cm<sup>-2</sup>.

The CV curves were also determined to calculate the double-layer capacitance (C<sub>dl</sub>) values of the HEO-O and HEO-900 samples, which were applied to investigate the electrochemical active surface area (ECSA) [37,38]. The CV curves were detected in the potential range of 0.75–0.85 V at the scanning rates from 10 mV s<sup>-1</sup> to 100 mV s<sup>-1</sup>, as shown in Figure 4a,b. The C<sub>dl</sub> values were calculated based on the CV curves, as shown in Figure 4c. It is noteworthy that the HEO-900 electrocatalyst contains a higher C<sub>dl</sub> value of 3.42 mF cm<sup>-2</sup> than that of HEO-O (1.38 mF cm<sup>-2</sup>). This result proves that the as-prepared sample of HEO-900 possesses a higher ECSA value, revealing the promoted exposure of OER active sites. Moreover, impedance is also a significant parameter for the electrocatalysts. As depicted in Figure 4d, the HEO-900 catalyst displayed a lower interface transfer impedance of 26.31 Ω than that of HEO-O (548.4 Ω), revealing the enhanced electron transfer. The low impedance is profitable for accelerating the OER process.

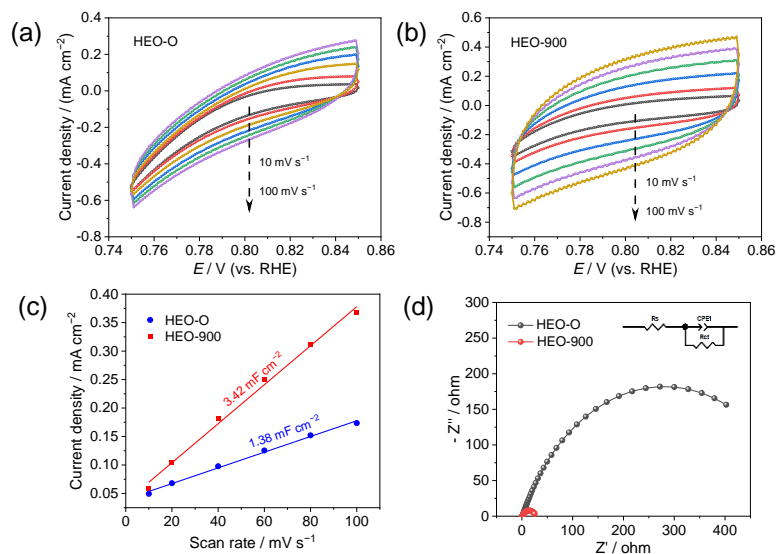


**Figure 4.** CV curves for (a) HEO-O and (b) HEO-900 at the scanning rates from 10 mV s<sup>-1</sup> to 100 mV s<sup>-1</sup>. (c) C<sub>dl</sub> values at various scanning rates. (d) Nyquist plots of HEO-O and HEO-900.

### 3.3. Catalytic Mechanism Analysis

In order to deeply exploit the catalytic mechanism, the surface element compositions and valence states of the HEO-900 catalyst after the OER process were determined by the XPS technique. The XPS full spectra indicate the coexistence of Ni, Co, Fe, Mn, Cr, and O elements in the HEO-900 catalyst (Figure S1). The high-resolution spectra of Co 2p, Fe 2p, Mn 2p, Ni 2p, and Cr 2p revealed that the bivalent and trivalent metal ions are presented for Co, Fe, Ni, and Cr elements, while the bivalent and quadrivalent metal ions were obtained for the Mn element, as depicted in Figure 5a–e. The high-valence metal species of Ni<sup>3+</sup>, Co<sup>3+</sup>, Fe<sup>3+</sup>, Mn<sup>4+</sup> and Cr<sup>3+</sup> were generated on the surface of the HEO-900 electrocatalyst after the OER. Generally, the high-valence metal species favor the adsorption of OER intermediates and are regarded as highly active phases for the OER process [39,40]. Here, the abundant metal sites of Co<sup>3+</sup>, Fe<sup>3+</sup>, Mn<sup>4+</sup>, Ni<sup>3+</sup>, and Cr<sup>3+</sup> coexist on the HEO-900 catalyst surface, and their synergetic effect is conducive to enhancing the activity of OER. Thus, the spinel-type high-entropy oxides of (Co, Fe, Mn, Ni, Cr)<sub>3</sub>O<sub>4</sub> achieve excellent OER performances.

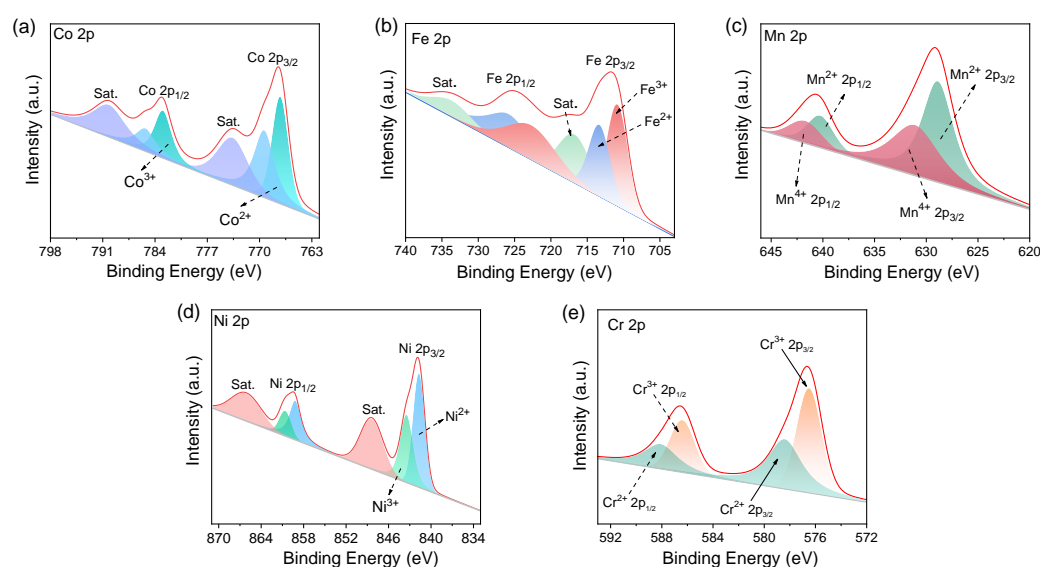


**Figure 5.** XPS spectra of HEO-900 after OER determination. (a) Co 2p spectrum. (b) Fe 2p spectrum. (c) Mn 2p spectrum. (d) Ni 2p spectrum. (e) Cr 2p spectrum.

### 4. Conclusions

In this work, we successfully synthesized the spinel-type high-entropy oxides of (Co, Fe, Mn, Ni, and Cr)<sub>3</sub>O<sub>4</sub> through the high-temperature calcination approach. The effect of calcination temperatures on structures and properties was investigated systematically. It is noteworthy that the optimized catalyst of HEO-900 contains the hybrid structure of regular polyhedrons and irregular nanoparticles, which is beneficial for the exposure of electrochemically active sites. Owing to the synergistic effect of the multi-metal sites, the as-prepared HEO-900 catalyst indicates excellent OER activity and needs the overpotential of 366 mV to reach the current density of 10 mA cm<sup>-2</sup>. In addition, the HEO-900 catalyst exhibits the prominent durability of running for 24 h at the current density of 10 mA cm<sup>-2</sup> with clear delay. Therefore, this work supplies a promising route for preparing high-performance multi-metal OER electrocatalysts for application in water electrocatalysis.

**Supplementary Materials:** The following supporting information can be downloaded at: <https://www.mdpi.com/article/10.3390/ma17143415/s1>, Figure S1: XPS full spectrum of HEO-900 after the OER determination; Table S1: Comparison of OER performances of HEO-900 with the recently reported catalysts.

**Author Contributions:** Conceptualization, X.H. and X.L.; methodology, R.W., X.T., and X.Z.; formal analysis, X.Z. and Z.W.; resources, R.W. and Z.W.; software, X.T. and D.Y.; writing—original draft preparation, X.H.; writing—review and editing, X.L. and D.Y.; project administration, X.L. All authors have read and agreed to the published version of the manuscript.

**Funding:** Project supported by the Joint Funds of National Natural Science Foundation of China (Grant No. U22A20130) and the Central Government Guides Local Science and Technology Development Projects of China (Grant No. 216Z4101G).

**Institutional Review Board Statement:** Not applicable.

**Informed Consent Statement:** Not applicable.

**Data Availability Statement:** The data presented in this study are available upon request from the corresponding author.

**Conflicts of Interest:** The authors declare no conflicts of interest.

## References

1. Du, J.; You, S.; Li, X.; Tang, B.; Jiang, B.; Yu, Y.; Cai, Z.; Ren, N.; Zou, J. In Situ Crystallization of Active NiOOH/CoOOH Heterostructures with Hydroxide Ion Adsorption Sites on Velutipes-like CoSe/NiSe Nanorods as Catalysts for Oxygen Evolution and Cocatalysts for Methanol Oxidation. *ACS Appl. Mater. Interfaces* **2020**, *12*, 686–697. <https://doi.org/10.1021/acsami.9b16626>.
2. Park, S.H.; Kang, S.H.; Youn, D.H. Direct One-Step Growth of Bimetallic Ni<sub>2</sub>Mo<sub>3</sub>N on Ni Foam as an Efficient Oxygen Evolution Electrocatalyst. *Materials* **2021**, *14*, 4768. <https://doi.org/10.3390/ma14164768>.
3. Yan, Z.; Guo, S.; Tan, Z.; Wang, L.; Li, G.; Tang, M.; Feng, Z.; Yuan, X.; Wang, Y.; Cao, B. Research Advances of Non-Noble Metal Catalysts for Oxygen Evolution Reaction in Acid. *Materials* **2024**, *17*, 1637. <https://doi.org/10.3390/ma17071637>.
4. Hwang, S.; Chen, X.; Zhou, G.; Su, D. In Situ Transmission Electron Microscopy on Energy-Related Catalysis. *Adv. Energy Mater.* **2019**, *10*, 1902105. <https://doi.org/10.1002/aenm.201902105>.
5. Pan, K.; Zhai, Y.; Zhang, J.; Yu, K. FeS<sub>2</sub>/C Nanowires as an Effective Catalyst for Oxygen Evolution Reaction by Electrolytic Water Splitting. *Materials* **2019**, *12*, 3364. <https://doi.org/10.3390/ma12203364>.
6. Gorlin, M.; Chernev, P.; Paciok, P.; Tai, C.W.; Ferreira de Araujo, J.; Reier, T.; Heggen, M.; Dunin-Borkowski, R.; Strasser, P.; Dau, H. Formation of unexpectedly active Ni-Fe oxygen evolution electrocatalysts by physically mixing Ni and Fe oxyhydroxides. *Chem. Commun.* **2019**, *55*, 818–821. <https://doi.org/10.1039/c8cc06410e>.
7. Liu, X.; Guo, X.; Gong, M.; Deng, S.; Liang, J.; Zhao, T.; Lu, Y.; Zhu, Y.; Zhang, J.; Wang, D. Corrosion-assisted large-scale production of hierarchical iron rusts/Ni(OH)<sub>2</sub> nanosheet-on-microsphere arrays for efficient electrocatalysis. *Electrochim. Acta* **2020**, *353*, 136478. <https://doi.org/10.1016/j.electacta.2020.136478>.
8. Sun, Y.; Zhang, T.; Li, C.; Xu, K.; Li, Y. Compositional engineering of sulfides, phosphides, carbides, nitrides, oxides, and hydroxides for water splitting. *J. Mater. Chem. A* **2020**, *8*, 13415–13436. <https://doi.org/10.1039/d0ta05038e>.
9. Fan, R.; Mu, Q.; Wei, Z.; Peng, Y.; Shen, M. Atomic Ir-doped NiCo layered double hydroxide as a bifunctional electrocatalyst for highly efficient and durable water splitting. *J. Mater. Chem. A* **2020**, *8*, 9871–9881. <https://doi.org/10.1039/d0ta03272g>.
10. Li, Y.; Li, F.; Meng, X.; Li, S.; Zeng, J.; Chen, Y. Ultrathin Co<sub>3</sub>O<sub>4</sub> Nanomeshes for the Oxygen Evolution Reaction. *ACS Catal.* **2018**, *8*, 1913–1920. <https://doi.org/10.1021/acscatal.7b03949>.
11. Kim, B.; Kim, T.; Lee, K.; Li, J. Recent Advances in Transition Metal Phosphide Electrocatalysts for Water Splitting under Neutral pH Conditions. *ChemElectroChem* **2020**, *7*, 3578–3589. <https://doi.org/10.1002/celec.202000734>.
12. Zhang, C.; Pu, Z.; Amiin, I.S.; Zhao, Y.; Zhu, J.; Tang, Y.; Mu, S. Co<sub>2</sub>P quantum dot embedded N, P dual-doped carbon self-supported electrodes with flexible and binder-free properties for efficient hydrogen evolution reactions. *Nanoscale* **2018**, *10*, 2902–2907. <https://doi.org/10.1039/c7nr08148k>.
13. Amiin, I.S.; Pu, Z.; Liu, X.; Owusu, K.A.; Monestel, H.G.R.; Boakye, F.O.; Zhang, H.; Mu, S. Multifunctional Mo-N/C@MoS<sub>2</sub> Electrocatalysts for HER, OER, ORR, and Zn-Air Batteries. *Adv. Funct. Mater.* **2017**, *27*, 1702300. <https://doi.org/10.1002/adfm.201702300>.
14. He, D.; Wu, X.; Liu, W.; Lei, C.; Yu, C.; Zheng, G.; Pan, J.; Lei, L.; Zhang, X. Co<sub>1-x</sub>S embedded in porous carbon derived from metal organic framework as a highly efficient electrocatalyst for oxygen evolution reaction. *Chin. Chem. Lett.* **2019**, *30*, 229–233. <https://doi.org/10.1016/j.ccl.2018.03.020>.
15. Keerthana, S.; Rani, B.J.; Yuvakkumar, R.; Ravi, G.; Hong, S.I.; Saravanakumar, B.; Velauthapillai, D.; Al-Mohaimed, A.M.; Algarni, T.S. Electrochemical Oxygen Evolution Reaction Activity of Tin Sulfide Nanostructures. *ChemistrySelect* **2020**, *5*, 11703–11707. <https://doi.org/10.1002/slct.202002495>.

16. Guo, Y.; Yuan, P.; Zhang, J.; Xia, H.; Cheng, F.; Zhou, M.; Li, J.; Qiao, Y.; Mu, S.; Xu, Q. Co<sub>2</sub>P-CoN double active centers confined in N-doped carbon nanotube: Heterostructural engineering for trifunctional catalysis toward HER, ORR, OER, and Zn-air batteries driven water splitting. *Adv. Funct. Mater.* **2018**, *28*, 1805641. <https://doi.org/10.1002/adfm.201805641>.
17. Xiong, B.; Ge, L.; Lei, X.; Wang, Y.; Yang, J.; Li, W.; Li, X.; Cheng, Z.; Fu, Z.; Lu, Y. Tailoring the electronic structure of ZnCo<sub>2</sub>O<sub>4</sub> by incorporating anions with low electronegativity to improve the water oxidation activity. *Sci. China Mater.* **2023**, *66*, 1793–1800. <https://doi.org/10.1007/s40843-022-2335-1>.
18. Yue, X.; Qin, X.; Chen, Y.; Peng, Y.; Liang, C.; Feng, M.; Qiu, X.; Shao, M.; Huang, S. Constructing Active Sites from Atomic-Scale Geometrical Engineering in Spinel Oxide Solid Solutions for Efficient and Robust Oxygen Evolution Reaction Electrocatalysts. *Adv. Sci.* **2021**, *8*, 2101653. <https://doi.org/10.1002/advs.202101653>.
19. Zhao, Q.; Yan, Z.; Chen, C.; Chen, J. Spinel: Controlled Preparation, Oxygen Reduction/Evolution Reaction Application, and Beyond. *Chem. Rev.* **2017**, *117*, 10121–10211. <https://doi.org/10.1021/acs.chemrev.7b00051>.
20. Liu, X.; Gong, M.; Xiao, D.; Deng, S.; Liang, J.; Zhao, T.; Lu, Y.; Shen, T.; Zhang, J.; Wang, D. Turning waste into treasure: Regulating the oxygen corrosion on Fe foam for efficient electrocatalysis. *Small* **2020**, *16*, 2000663. <https://doi.org/10.1002/smll.202000663>.
21. Xie, J.; Xin, J.; Wang, R.; Zhang, X.; Lei, F.; Qu, H.; Hao, P.; Cui, G.; Tang, B.; Xie, Y. Sub-3 nm pores in two-dimensional nanomesh promoting the generation of electroactive phase for robust water oxidation. *Nano Energy* **2018**, *53*, 74–82. <https://doi.org/10.1016/j.nanoen.2018.08.045>.
22. Yao, M.; Hu, H.; Wang, N.; Hu, W.; Komarneni, S. Quaternary (Fe/Ni)(P/S) mesoporous nanorods templated on stainless steel mesh lead to stable oxygen evolution reaction for over two months. *J. Colloid Interf. Sci.* **2020**, *561*, 576–584. <https://doi.org/10.1016/j.jcis.2019.11.032>.
23. Yu, F.; Zhou, H.; Huang, Y.; Sun, J.; Qin, F.; Bao, J.; Goddard, W.A., 3rd; Chen, S.; Ren, Z. High-performance bifunctional porous non-noble metal phosphide catalyst for overall water splitting. *Nat. Commun.* **2018**, *9*, 2551. <https://doi.org/10.1038/s41467-018-04746-z>.
24. Zhang, N.; Feng, X.; Rao, D.; Deng, X.; Cai, L.; Qiu, B.; Long, R.; Xiong, Y.; Lu, Y.; Chai, Y. Lattice oxygen activation enabled by high-valence metal sites for enhanced water oxidation. *Nat. Commun.* **2020**, *11*, 4066. <https://doi.org/10.1038/s41467-020-17934-7>.
25. Park, H.; Park, B.H.; Choi, J.; Kim, S.; Kim, T.; Youn, Y.-S.; Son, N.; Kim, J.H.; Kang, M. Enhanced electrochemical properties and OER performances by Cu substitution in NiCo<sub>2</sub>O<sub>4</sub> spinel structure. *Nanomaterials* **2020**, *10*, 1727. <https://doi.org/10.3390/nano10091727>.
26. Lee, S.; Kim, S.; Jang, Y.; Park, J.; Byeon, J.; Lee, J. Oxophilicity induced surface hydroxylation to promote oxygen evolution in selectively substituted spinel-type cobalt oxides. *J. Phys. Chem. C* **2023**, *127*, 15062–15068. <https://doi.org/10.1021/acs.jpcc.3c02867>.
27. Vazhayil, A.; Ashok, C.S.; Thomas, N. Probing the electrocatalytic activity of hierarchically mesoporous M-Co<sub>3</sub>O<sub>4</sub> (M = Ni, Zn, and Mn) with branched pattern for oxygen evolution reaction. *J. Electroanal. Chem.* **2023**, *934*, 117298. <https://doi.org/10.1016/j.jelechem.2023.117298>.
28. Qi, C.; Liu, Q.; Dong, Y.; Zhang, G.; Jiang, X.; Gao, D. Quenching-induced surface reconstruction of FeMn<sub>2</sub>O<sub>4</sub> for promoted oxygen evolution reaction. *J. Alloys Compd.* **2023**, *967*, 171754. <https://doi.org/10.1016/j.jallcom.2023.171754>.
29. Huang, X.; Wang, X.; Liu, Y.; Hou, Y.; Li, C.; Cai, M.; Gu, H.; Cao, X. General synthesis of CoCeMO<sub>x</sub> trimetallic oxides via a cation exchange reaction for the oxygen evolution reaction. *Dalton Trans.* **2023**, *52*, 5312–5320. <https://doi.org/10.1039/D3DT00318C>.
30. Guo, S.; Wang, X.; Zhou, X.; Li, H.; Ding, X. Tuning oxygen vacancies in Co<sub>3</sub>O<sub>4</sub> nanorods through solvent reduction method for enhanced oxygen evolution activity. *Energy Fuels* **2023**, *37*, 5421–5428. <https://doi.org/10.1021/acs.energyfuels.3c00034>.
31. Sultan, F.; González Sepúlveda, G.E.; Medina, D.I.; Videa, M.; Sánchez-Domínguez, M.; Cholula-Díaz, J.L. Synthesis of MFe<sub>2</sub>O<sub>4</sub> (M = Ni, Co) nanoparticles by a bicontinuous microemulsion method for the oxygen evolution reaction. *ChemNanoMat* **2024**, *10*, e202300541. <https://doi.org/10.1002/cnma.202300541>.
32. Shoaib, M.; Qiao, F.; Xu, X.; Zhou, T.; Liu, Y. Influence of Mo concentration on the structural and electrochemical properties of double-doped Mo-Co-Ni<sub>3</sub>S<sub>2</sub>/NF composites. *CrystEngComm* **2024**, *26*, 1884–1891. <https://doi.org/10.1039/D3CE01246H>.
33. Kayış, Z.; Akyüz, D. A high-performance electrocatalyst via graphitic carbon nitride nanosheet-decorated bimetallic phosphide for alkaline water electrolysis. *Phys. Chem. Chem. Phys.* **2024**, *26*, 14908–14918. <https://doi.org/10.1039/D4CP00020J>.
34. Zhao, L.; Liu, S.; Wei, L.; He, H.; Jiang, B.; Zhan, Z.; Wang, J.; Li, X.; Gou, W. One-pot hydrothermal synthesis of bifunctional Co/Mo-rGO efficient electrocatalyst for HER/OER in water splitting. *Catal. Lett.* **2024**. <https://doi.org/10.1007/s10562-024-04723-w>.
35. Li, W.; Xu, H.; Pei, Y.; Hu, L.; Yang, Z. Investigation into the performance of tremella-like LaNiO<sub>3</sub>-NiO composite as an electrocatalyst for oxygen evolution reaction. *Ionics* **2024**. <https://doi.org/10.1007/s11581-024-05614-1>.
36. Wang, L.; Li, J.; Li, Y.; Dong, X.; Shan, H.; Chen, S.; Sun, P.; Zhang, F.; Li, W.; Chu, X.; et al. Cobalt-based transition metal boride electrocatalysts for alkaline water oxidation reactions. *Ionics* **2024**, *30*, 943–950. <https://doi.org/10.1007/s11581-023-05302-6>.
37. Ma, L.; Zhu, G.; Wang, D.; Chen, H.; Lv, Y.; Zhang, Y.; He, X.; Pang, H. Emerging Metal Single Atoms in Electrocatalysts and Batteries. *Adv. Funct. Mater.* **2020**, *30*, 2003870. <https://doi.org/10.1002/adfm.202003870>.
38. Zhao, K.; Ma, X.; Lin, S.; Xu, Z.; Li, L. Ambient Growth of Hierarchical FeOOH/MXene as Enhanced Electrocatalyst for Oxygen Evolution Reaction. *ChemistrySelect* **2020**, *5*, 1890–1895. <https://doi.org/10.1002/slct.201904506>.

39. Liu, X.; Gong, M.; Deng, S.; Zhao, T.; Zhang, J.; Wang, D. Recent advances on metal alkoxide-based electrocatalysts for water splitting. *J. Mater. Chem. A* **2020**, *8*, 10130–10149. <https://doi.org/10.1039/d0ta03044a>.
40. Gouda, L.; Sévery, L.; Moehl, T.; Mas-Marzá, E.; Adams, P.; Fabregat-Santiago, F.; Tilley, S.D. Tuning the selectivity of biomass oxidation over oxygen evolution on NiO-OH electrodes. *Green Chem.* **2021**, *23*, 8061–8068. <https://doi.org/10.1039/d1gc02031e>.

**Disclaimer/Publisher's Note:** The statements, opinions and data contained in all publications are solely those of the individual author(s) and contributor(s) and not of MDPI and/or the editor(s). MDPI and/or the editor(s) disclaim responsibility for any injury to people or property resulting from any ideas, methods, instructions or products referred to in the content.